Understanding galling wear initiation and progression using force and acoustic emissions sensors

Shanbhag, V. V., Rolfe, B. F., Griffin, J. M., Arunachalam, N. & Pereira, M. P.

Author post-print (accepted) deposited by Coventry University's Repository

Original citation & hyperlink:
Shanbhag, VV, Rolfe, BF, Griffin, JM, Arunachalam, N & Pereira, MP 2019, 'Understanding galling wear initiation and progression using force and acoustic emissions sensors', Wear, vol. 436-437, 202991.
https://dx.doi.org/10.1016/j.wear.2019.202991

DOI 10.1016/j.wear.2019.202991
ISSN 0043-1648
ESSN 1873-2577

Publisher: Elsevier

NOTICE: this is the author's version of a work that was accepted for publication in *Wear*. Changes resulting from the publishing process, such as peer review, editing, corrections, structural formatting, and other quality control mechanisms may not be reflected in this document. Changes may have been made to this work since it was submitted for publication. A definitive version was subsequently published in *Wear*, 436-437, (2019) DOI: 10.1016/j.wear.2019.202991

© 2019, Elsevier. Licensed under the Creative Commons Attribution-NonCommercial-NoDerivatives 4.0 International http://creativecommons.org/licenses/by-nc-nd/4.0/

Copyright © and Moral Rights are retained by the author(s) and/ or other copyright owners. A copy can be downloaded for personal non-commercial research or study, without prior permission or charge. This item cannot be reproduced or quoted extensively from without first obtaining permission in writing from the copyright holder(s). The content must not be changed in any way or sold commercially in any format or medium without the formal permission of the copyright holders.

This document is the author's post-print version, incorporating any revisions agreed during the peer-review process. Some differences between the published version and this version may remain and you are advised to consult the published version if you wish to cite from it.

Journal Pre-proof

Understanding galling wear initiation and progression using force and acoustic emissions sensors

VigneshV. Shanbhag, Bernard F. Rolfe, James M. Griffin, Narayanan Arunachalam, Michael P. Pereira

PII: S0043-1648(19)30331-X

DOI: https://doi.org/10.1016/j.wear.2019.202991

Reference: WEA 202991

To appear in: *Wear*

Received Date: 11 February 2019

Revised Date: 27 July 2019

Accepted Date: 28 July 2019

Please cite this article as: V. Shanbhag, B.F. Rolfe, J.M. Griffin, N. Arunachalam, M.P. Pereira, Understanding galling wear initiation and progression using force and acoustic emissions sensors, *Wear* (2019), doi: https://doi.org/10.1016/j.wear.2019.202991.

This is a PDF file of an article that has undergone enhancements after acceptance, such as the addition of a cover page and metadata, and formatting for readability, but it is not yet the definitive version of record. This version will undergo additional copyediting, typesetting and review before it is published in its final form, but we are providing this version to give early visibility of the article. Please note that, during the production process, errors may be discovered which could affect the content, and all legal disclaimers that apply to the journal pertain.

© 2019 Published by Elsevier B.V.

Journal Pre-proof

Title Page

Paper title:

Understanding galling wear initiation and progression using force and acoustic emissions sensors

Author Names:

Vignesh.V.Shanbhag[1*], Bernard. F.Rolfe [2], James. M. Griffin [3], Narayanan Arunachalam [4], Michael. P.Pereira[2]

Author Affiliations:

[1] Institute for Frontier Materials, Deakin University, Waurn Ponds, VIC, 3216, Australia
[2] School of Engineering, Deakin University, Waurn Ponds, VIC, 3216, Australia
[3] Institute for Future Transport and Cities, Coventry University, Coventry, UK, CV1 5FB
[4] Mechanical Engineering Department, Indian Institute of Technology Madras, India, 600036

Corresponding Author*:

Vignesh Shanbhag

Email ID: vshanbha@deakin.edu.au

Institute for Frontier Materials, Deakin University, Waurn Ponds, VIC, 3216, Australia

Journal Pre-proof

Journal Pre-proof

Understanding galling wear initiation and progression using force and acoustic emissions sensors

Highlights

- AE peak feature can be used to study initiation of galling.
- Tangential force can be used to indicate prior indication of galling.
- Indenter attack angle plays an important role on the abrasive wear transition.
- Profile depth is quantitative wear measurement to study abrasive wear transition.

Abstract

In the stamping process, tools are prone to an adhesive wear mode called galling. This galling wear mode on the stamping tool results in an abrasive wear modes like ploughing and cutting on the workpiece. To study the adhesive and abrasive wear modes relevant in sheet metal stamping processes, scratch tests were performed under controlled conditions where galling, ploughing and cutting can be observed. Two sets of scratch tests were performed to study the galling behaviour using force and acoustic emission sensors. In the first test set, scratch tests were performed at a different depth of penetration to segregate the non-galling and galling conditions. In the second test set, scratch tests were performed at a different sliding distances to understand the influence of galling on the abrasive wear modes. To study the galling behaviour, acoustic emission and force features from both of the test sets were correlated with profilometry wear measurement features like profile depth, wear index, attack angle and volume measurement of galling. From the quantitative measurement of galling on the indenter, a minimal lump was observed on the indenter when the cutting at the edges of scratch was observed. A much larger lump was observed on the indenter for conditions when fracture was observed on the workpiece at the centre of the scratch. The acoustic emission burst signal and unstable force behaviour was mainly observed when the signicant lump was observed on the indenter. The methodology adopted to investigate galling wear in this study lays the strong foundation to develop real-time monitoring systems to observe the transition from non-galling to galling conditions.

Keywords: Galling, Ploughing, Cutting, Acoustic emissions, Force, Profile depth, Attack angle.

1. Introduction

The continued focus on vehicle weight reduction in the automotive industry has resulted in the increased use of advanced and ultra-high strength steels in car body panels. This has led to increased forming forces and stresses on the stamping tools used in automotive manufacturing, leading to premature failure of the stamping tools [1]. In dry and low lubrication forming conditions – especially for uncoated cast iron and steel tools – failure of the tooling is primarily attributed to an adhesive wear mechanism called galling. According to ASTM G40-17 [2], galling wear is a form of surface damage arising between sliding solids, distinguished by macroscopic, usually localized, roughening and creation of protrusions above the original surface. The protrusion due to galling wear results in plastic flow or material transfer, or both [2]. In sheet metal stamping process, galling occurs between sliding surfaces, due to surface defects, inefficiency of lubricants and the temperature at tool workpiece interface and results in the transfer of sheet material to the tool surface. This transferred material can then become work hardened and result in large hard protrusions on the tool surfaces, which can then cause severe scratching of the opposing sheet surfaces [3-4]. This scratching mechanism on the sheet surface can be considered as abrasive wear modes [5-7]. The most common abrasive wear modes are two and three body abrasive wear modes. According to ASTM G40-17 [2], in two body abrasive wear, the hard particles which produce the wear of one body are fixed on the surface of other body. This two body abrasive wear often changes to three body abrasive wear as the wear debris acts as abrasives between two solid bodies in relative motion [2, 9]. The most common type of abrasive wear that are observed in sheet metal stamping process are ploughing and cutting wear [6-8]. Ploughing can be defined as the formation of grooves due to plastic deformation of the softer surface between the two surfaces in relative motion. Whereas, during cutting wear, material is taken away in the form of debris [2, 9]. In sheet metal stamping process, these scratches on the sheet surface can develop very quickly due to the rapid build-up of transferred material during the growth stage of the galling mechanism [8]. This results in the need for regular maintenance of the stamping tools or unscheduled stoppages in production due to wear-induced

deterioration of part surface quality. In these cases, even a slight improvement in the tool maintenance method, via an improved understanding of the instantaneous state of the tools, can reduce machine downtime and unscheduled maintenance. Therefore, monitoring of tool wear in real-time in industry is of high importance, and can provide significant benefit compared to other wear measurement methods (e.g. mass loss, visual inspection, surface profilometry), since these methods do not provide timely information about possible transition in wear mechanisms and the severity of any localised wear at the tool-workpiece interface.

Galling initiation has been studied in sheet metal forming using different experimental setups and sensors. For example, considerable studies have been performed to study galling development on the tool using force sensors. Gåård et al. [3], Karlsson et al. [4] and Heidi et al. [10] investigated the galling resistance using force sensors on slider on sheet tribology tests. In these studies, the force was observed to be unstable when galling was observed and the presence of galling was indicated by qualitative observation of the tool and sheet surfaces. Galling initiation was found to result in an increment in the measured tangential force [3, 11]. In addition to galling wear on the tools, Gåård et al. [3] and Karlsson et al. [4] also observed abrasive wear on the sheet surface due to the presence of galling on the tool surface. As the galling initiation on the tool and sheet surface, was indicated qualitatively in these studies, therefore it is evident that there has been limited attempts made to correlate the force behaviour due to galling initiation with the quantitative wear measurement of tool and sheet surface. Therefore, there is a need for additional studies to understand the force behaviour due to non-galling conditions and galling conditions, by quantitatively measuring the galling and its progression on the tool surface and wear on the sheet surface.

Adhesive and abrasive wear have been studied together using a single experimental setup. For example, Hase et al. [12] used an acoustic emission (AE) sensor during pin on block tests using two different material conditions and found adhesive or abrasive wear, depending on the material pairs examined. To investigate adhesive wear, the material combination of a metal pin and metal block was used and adhesive wear was observed in the AE frequency range of 1-1.5 MHz. To investigate abrasive wear, the material combination of an iron pin and emery paper was used and abrasive wear was observed in the AE frequency range of 0.3-1 MHz [12]. To investigate adhesive and abrasive wear within a single set of test conditions and material combination, Sindi et al. [13] used an AE sensor on the slider on sheet setup with a material combination of tool steel and stainless steel and observed severe scratches and adhesive wear in the AE frequency range of 0.19-0.375 MHz. The AE features were qualitatively correlated with the surface images of the workpiece. As observed in the study of Hase et al. [12] and Sindi et al. [13], only the AE burst signals were used for the analysis and the results were focussed on the behaviour after abrasive wear had been observed on the sheet surface due to adhesive wear on the tool surface. However, to understand the transition from non-galling to galling conditions, there is a need for additional investigation using the continuous AE data recording and to analyse how the AE signal changes during this transition. This knowledge will be a key step towards developing AE-based real-time monitoring tools and, therefore, forms the basis for the work in this paper.

There have also been considerable attempts to investigate the galling wear under the industrial conditions. For example, Ubhayaratne et al. [1] studied galling initiation in a sheet metal stamping process using the audio sensor and by examining the worn condition of the sheet surfaces using optical profilometer measurements. Voss et al. [14] developed a methodology using optical profilometer wear measurement to detect and measure galling in sheet metal stamping wear tests by performing the wavelet analysis on the surface profiles of the sheet surface. Skåre et al. [15] and Shanbhag et al. [16] also investigated the galling initiation on the tool using AE sensors in similar semi-industrial sheet metal stamping tests. Shanbhag et al. [16] also investigated the galling wear using a “profile depth” wear measurement feature obtained from the surface profiles of the sheet surface. In all these studies, the presence of galling was indicated by the surface examination of the workpiece. However, in the literature, there is very little work that attempts to quantitatively measure and understand the wear mechanism on the sheet surface and wear mechanism on the tool, possibly due to the difficulty in obtaining detailed measurements of both surfaces at sufficiently regular intervals during the industrial-type test conditions. Therefore, there is a need to perform tests under controlled conditions using the same material combinations which permits the investigation of the wear mechanism on tool and the sheet surface. For this reason, scratch tests have been widely used to study only the abrasive wear modes [17-19] and also to study the combination of abrasive wear and adhesive wear modes [20-21] under controlled conditions. The transition of abrasive wear from the ploughing mode to the cutting mode is dependent on the surface conditions of the tool. A lump growth model was developed by de Rooij et al. [22-23] to explain the galling initiation on the tool during the wedge formation abrasive wear mode. However, there is need for experimental confirmation by quantitatively measuring the lump on the tool during the wedge formation mode. In addition, there has been little study or no attempt made to actively monitor the galling development during the abrasive wear transition (ploughing to cutting) using force and AE and understand how the force and AE signals change with the galling progression.

Journal Pre-proof

Since force and AE sensors have been successfully used to investigate galling, this study investigates the influence of galling wear of the indenter on the abrasive wear mechanisms using a combination of force and AE sensors. To understand the transition from non-galling to galling wear mechanisms, a series of experiments were performed in controlled conditions using a scratch tester. Two sets of experiments were performed to meet the objective. In the first set, the experiments were performed to understand the conditions that caused galling (compared to non-galling conditions). In the second set, the experiments were performed to understand the initiation and evolution of galling on the indenter and its influence on the abrasive wear mechanisms that occur on the counter (workpiece) surface.

2. Experimental details

2.1 Scratch test setup

Displacement controlled scratch tests were performed based on a custom setup developed using a semi-automatic turret milling machine (supplier: HAFCO MetalMaster; Product label BM23A). Scratch tests were adopted in this study due to number of advantages, such as the ability: (a) to investigate galling under short sliding distance using controlled depth of penetration settings; (b) to allow continuous recording of AE data under high AE sampling frequency; (c) to allow surface examination of the workpiece samples under optical profilometer to quantify wear features versus sliding distance, which can permit the correlation with measured AE and force features and measured lump growth on the indenter. The tests were performed in the y-direction as shown in Fig. 1. During the test, the rotation of the spindle was locked and the speed (feed rate) was maintained constant. A Kistler dynamometer was attached to the bed of the milling machine using clamps and flange nuts. The blank material (165 mm long × 100mm wide × 2 mm thick) was bolted to the dynamometer. The indenter was conical (30° cone, 10 mm shaft diameter) with a spherical tip (1.5 mm radius).

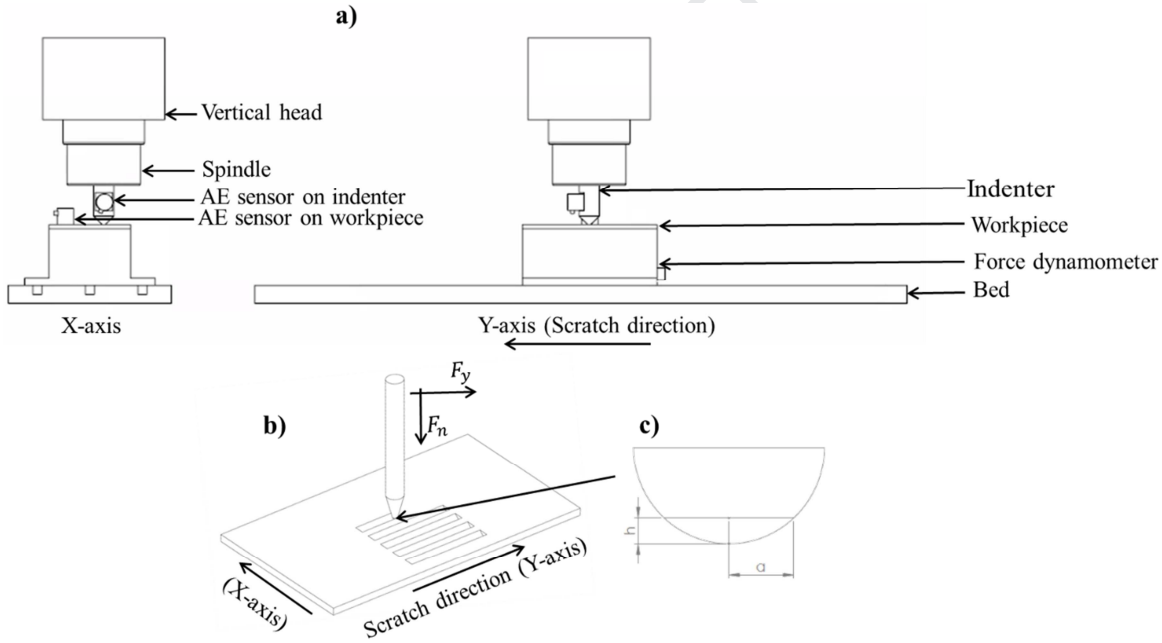

Fig. 1. Schematic view of: a) scratch test setup, b) scratch orientation and c) parameters for depth of penetration measurement.

The tests were performed in two main test sets under dry conditions, as summarized in Table 1. For Test Set 1, the tests were performed at a different depth of penetration, D_p (Equation 1). Six tests were conducted at varying D_p to study non-galling and galling conditions. For Test Set 2, experiments were performed at varying sliding distances and constant D_p. Six tests were conducted at varying sliding distances to study development of galling on the indenter and its influence on abrasive wear modes. The methodology described by Hokkirigawa et al. [24] to calculate D_p was used. Before the start of each test, the indenter and sheet surfaces were cleaned by hand using ethanol and Kimwipes. Dry Kimwipes were again used to clean the indenter and sheet surface to ensure that the ethanol had been thoroughly cleaned from the surface of the samples after the cleaning process. After each test, the indenter was removed and the surface was inspected and measured. On the workpiece, a minimum distance of 5 mm between each scratch was used to ensure that there was no interference with the neighbouring scratch. To show the test-to-test repeatability of results obtained from the scratch test, the scratch tests were

Journal Pre-proof

repeated under two sets of the same D_p experimental conditions. The process parameters used for the repeatability studies are explained in Table 1.

$$Depth\ of\ peTetTatioT, D_{pT} = T\frac{HeightTof\ indentation\ (h)T}{ContactTwidth\ (a)T} \text{.....} (1)$$

Table 1: Experimental parameters

General test conditions		
Test condition	Dry	
Sheet material	DP 780	
Indenter material	Cemented carbide with 10% Co	
Speed [mm/s]	2.2-2.4	
AE recording frequency	2 MS/s per channel	
Number of AE sensors	2	
Test conditions for each set of tests		
Test set label	Test Set 1	Test Set 2
Aim of test set	Effect of D_p	Effect of Sliding Distance
Depth of penetration, D_p [-]	0.16, 0.18, 0.2, 0.22, 0.24, 0.26	0.22
Initial load during the test [N]	400, 600, 800, 100, 1200, 1400	1000
Sliding distance [mm]	30	5, 10, 15, 20, 25, 30
Test conditions for the Repeatability Tests		
D_p [-]	0.18 (Test 1, 2, 3) and 0.24 (Test 4, 5, 6, 7)	
Sliding distance [mm]	30	
Speed [mm/s]	2.1-2.3	

2.2 Materials

The material used for the indenter was cemented tungsten carbide (WC-10%Co). The material used for the workpiece was dual phase steel (supplier: Bluescope steel; grade: DP780) with a thickness of 2mm and hardness of 28HRC. This material is classified as an Advanced High Strength Steel (AHSS) grade and is typically used for automotive structural components such as pillars, crash rails and rocker panels. The average surface roughness, *Ra*, of the as-received sheet was measured to be 1.2µm. The yield strength and ultimate tensile strength of the workpiece in the rolling direction are 530 and 880 MPa, respectively, as measured by quasi-static tensile tests conducted at room temperature in accordance with Australian Standard AS 1391-1991. The chemical composition of DP780 was measured using glow-discharge optical emission spectroscopy technique (GD-OES) and the results are presented in Table 2.

Table 2: Chemical composition of DP780

Chemical	Fe	C	Mn	Si	Al	Ni	Cr	N
% Weight	Balance	0.18	0.58	0.04	0.04	0.07	0.1	0.11

2.3 Data acquisition setup

Wear in the scratch test is observed on the indenter as well as on the workpiece [5]. Therefore, as shown in Fig. 1, two wideband AE sensors were used in this study (supplier: Vallen Systeme; model: AE2045S). The flat frequency response of these AE sensors is in the range of 0.2 to 2.5 MHz. One AE sensor was clamped on the indenter, just above the conical shape of the indenter, and the second AE sensor was clamped on the workpiece, as shown in Fig. 1. To increase the AE transmission, a small amount of ultrasonic couplant (supplier: Cordex; product label: UT 5000) was applied to the faces of the AE sensors and the AE sensors were clamped to the indenter and workpiece using screw clamps. Continuous AE data recording was performed for each test at 2 MHz per channel. The AE wideband sensors were connected to the data acquisition system (supplier: National Instruments, model: PXIe-1078) via a high-speed digitiser (supplier: National instruments, model: DCPL2) and an amplifier (supplier: Vallen Systeme; model: AEP3N) with a gain of 40dB. Due to the large file size, the AE data acquisition was stopped at the end of each test to allow the AE data to be recorded to the laptop (Lenovo T430).

A multicomponent dynamometer (triaxial force sensor load cell, supplier: Kistler; model: 9257B) was used to acquire tangential force during the scratch test. The dynamometer was connected to the laptop via a multi-channel charge amplifier (supplier: Kistler, Type: 5070A). The force data was acquired at a frequency of 5 kHz. The force data was pre-set to zero before the start of the scratch test, after the initial normal indentation into the workpiece surface.

2.4 Optical profilometry study

A 3D optical profilometer (equipment: Alicona-InfiniteFocus) was used to examine the surfaces of the indenter (before and after the tests) and the scratch on the workpiece. For all of the optical profilometer measurements, an objective magnification of 10× was used. To obtain the 3D data set for the entire scratch and indenter surface, the special resolution was set to 20 µm for the workpiece and 1.8 µm for the indenter. As-rolled sheets were used for the scratch test, therefore curvature and tilt removal were applied to the workpiece data using the plane feature available in the profilometer software to remove any uneven flatness and to level the surface (IF-MeasurementSuite v.5.1) [25].

2.4.1 Workpiece surface measurement

To quantify the wear on the scratch surface, two types of wear measurement were performed using the optical profilometry measurements: profile depth and wear index. The wear index can be used to indicate the abrasive wear mechanisms that occur during the scratch test [24]. Additionally, profile depth has shown a close correlation with AE measurements [7, 16]. Therefore, the profile depth was measured along the scratch direction at the centre and at the edges of the scratch as shown in Fig. 2. The width of the profile depth measurement at the centre of scratch and at the edges of the scratch is 0.5 and 0.2 mm respectively (Fig. 2-c). The start and end of the scratch (1 mm length) were discarded for the profile depth measurements to avoid the influence on the indenter loading and unloading on the beginning and end of the scratch tests profiles.

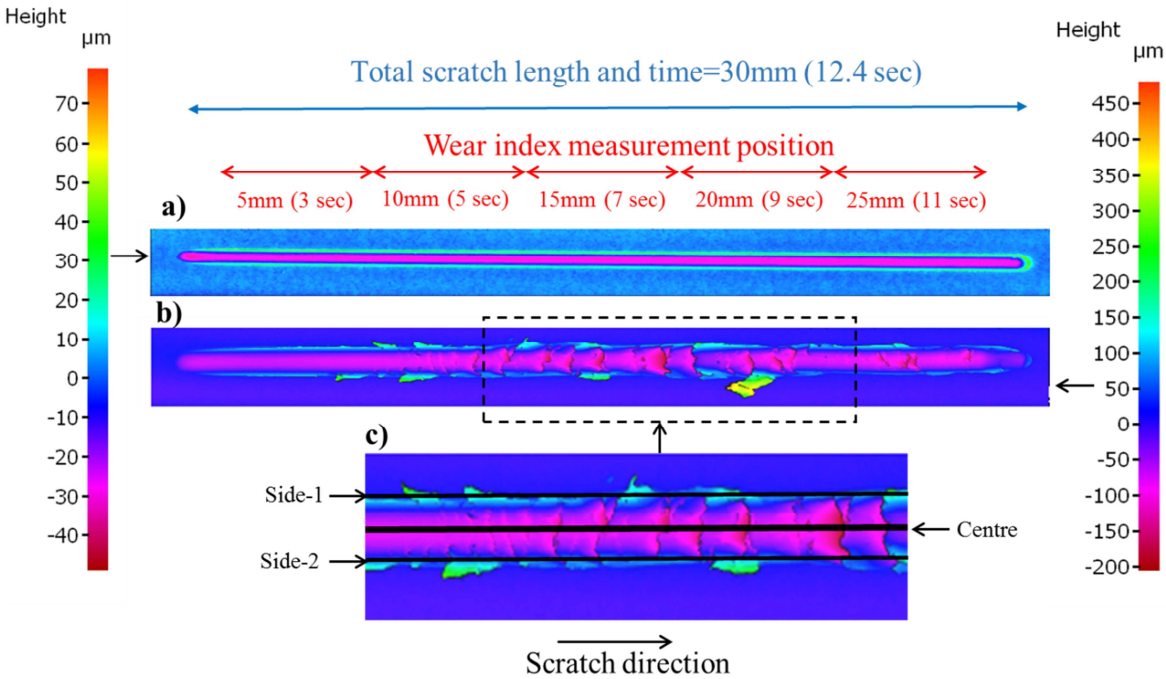

Fig. 2. Explanation of profilometry measurements of workpiece after scratch tests. Surface contours of the scratch for the following conditions: a) D_p =0.18 b) D_p =0.26. c) Location of the profile depth measurements.

As shown in Fig. 2, the wear index was calculated by taking the average transverse profile over 5 mm scratch length intervals along the scratch direction, to understand how the abrasive wear mechanisms changed during the scratch test. The method to calculate wear index described by Hokkirigawa et al. [24] was used and is summarised in Fig. 3 and Equations 2, 3 and 4. As shown in Fig. 2, the start and end of the scratches (2.5 mm) were not used in the wear index calculations due to the possible unsteady conditions at the beginning and end of the tests caused by machine start-up and finish and due to the indentation and unloading conditions experienced at these regions. Therefore, for the 30mm scratch length tests, five transverse surface profiles were obtained (each profile obtained by averaging the profile along a 5 mm scratch length), as shown in Fig. 2. Due to the short sliding length for the 5 mm scratch length test in Test Set 2, the wear index was calculated for an interval

of 3mm and only 1mm at the start and end of scratch were discarded. The reference line of each of the surface profile as shown in Fig. 3 was nearly horizontal. This reference line was used to segregate an area of ridges and apparent groove area. The area of the ridges and apparent groove was calculated using the function "trapz" available in Matlab software [17, 26].

To show the reliability of the wear index measurement in this study, the wear index was also calculated for all the transverse surface profiles obtained from the new Reliability Tests. Furthermore, to show that profile measurement and wear index measurement procedure resulted in consistent results, the wear index calculations were conducted using a different 2.5 mm interval along the scratch direction (as well as the "standard" 5 mm interval shown in Fig. 2). This assessment of the possible measurement-to-measurement variation was conducted for two of the Repeatability Tests with the higher value of D_p (i.e. tests 4 and 6 with D_p 0.24) and the results will be shown in Fig. 11.

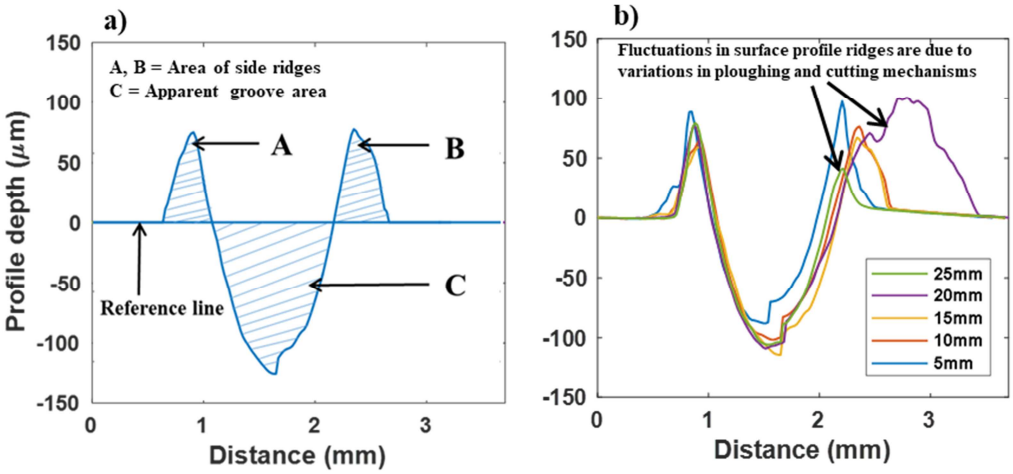

Fig. 3. a) Schematic of the transverse scratch profile used for wear index measurement. b) Example of the transverse surface profiles taken at different positions along the scratch length for D_p of 0.26. (Note that each profile is averaged over the 5 mm scratch length intervals shown in Fig. 2.)

$$otalTaTea\ ofT\ idges\ (A^1) = A + B \text{.....} (2)$$

$$Net\ gToove\ aTeaT(A^{11}) = A^1 - C \text{.....} (3)$$

$$WeaT\ i\ \ dexT=T\frac{GrooveTarea\ (A^{11})}{Apparent\ groove\ area\ (C)} \text{.....} (4)$$

2.4.2 Indenter surface measurement

2.4.2.1 Using optical profilometer

The surface of the indenter was measured after each test using the optical profilometer. The optical profilometry measurements were used to visually confirm the presence of galling, in a similar manner to other work in the literature [27]. For Test Set 2, the volume of the lump accumulated on the indenter was determined after each test so that the amount of galling could be quantified. The difference measurement tool in the optical profilometer equipment allows to compare two different geometries [25]. Therefore, the volume of the lump was determined by calculating the difference between the unworn and worn surfaces, using this difference measurement feature. The methodology adopted in this study for measuring volume of the lump via the optical profilometry is as follows:

a) Measure the unworn surface of indenter before test (Fig. 4-a);
b) Measure the worn surface of indenter after test (Fig. 4-b);
c) Using the difference measurement feature, manually move the worn surface measurement (Fig. 4-b) over the unworn (reference) surface in the 3D geometry space in the software;
d) Use the fit option to overlap the two surfaces to minimise the error between the two surface scans (Fig. 4-c); and
e) Calculate the volume above the reference surface to measure the debris/lump on the indenter – i.e. the volume of adhered material.

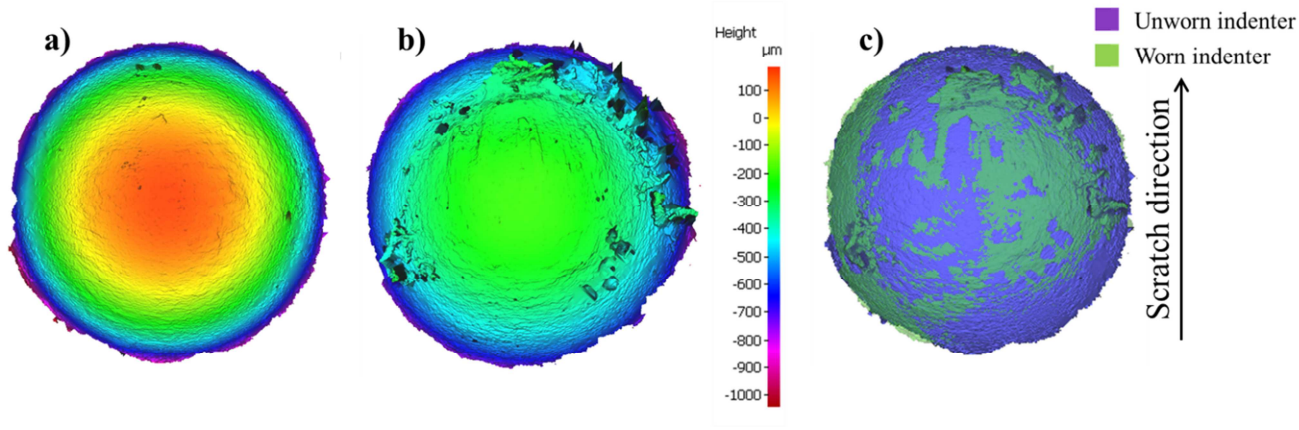

Fig. 4. Example profilometer contours of: a) the unworn indenter; b) the worn indenter (after the test of sliding distance 15mm, D_p=0.22); and c) overlapped indenter surface of the unworn and worn indenter, showing the difference between the two measurements.

2.4.2.2 Using Scanning Electron Microscope (SEM)

To confirm the presence of galling on indenter tip, the lump from the indenter tip (for Repeatability Test 1, D_p 0.24) was examined using SEM. The SEM measurements were conducted using a JEOL JSM-IT300 instrument, with a secondary electron mode of 20 kV, working distance of 10.8 mm and image resolution of 1024 X 832 pixels. Due to the height limitation of vacuum chamber in the SEM instrument, the galling lump from the indenter was manually mechanically removed from the indenter tip. The galling lump was later placed on the workpiece holder of the SEM instrument for SEM and EDX examination.

2.4.3 Attack angle estimation

The measurements of the surfaces of the indenter and workpiece after the tests were used to calculate the approximate attack angle at the end of the scratch tests. This estimate of the attack angle was used to understand the influence of a change in attack angle during the galling development, as it is known that attack angle between the hard asperity and the soft workpiece plays a key role in the resulting wear mechanisms [22-23]. As shown in Fig. 5-a, the longitudinal 2D profile on the workpiece was obtained by measuring a 0.2 mm wide centreline at the end of the scratch. On the obtained profile (Fig. 5-b), three points were selected to obtain two best fit lines. From the obtained best fit lines, the attack angle was measured (Fig. 5-b). A similar method was used to understand the location of adhered (galled) material on the indenter. As shown in Fig. 5-c, a straight line (0.2 mm wide) was selected on the worn indenter to obtain a longitudinal 2D profile of the indenter (Fig. 5-d) so that the location of the lump on the indenter could be examined.

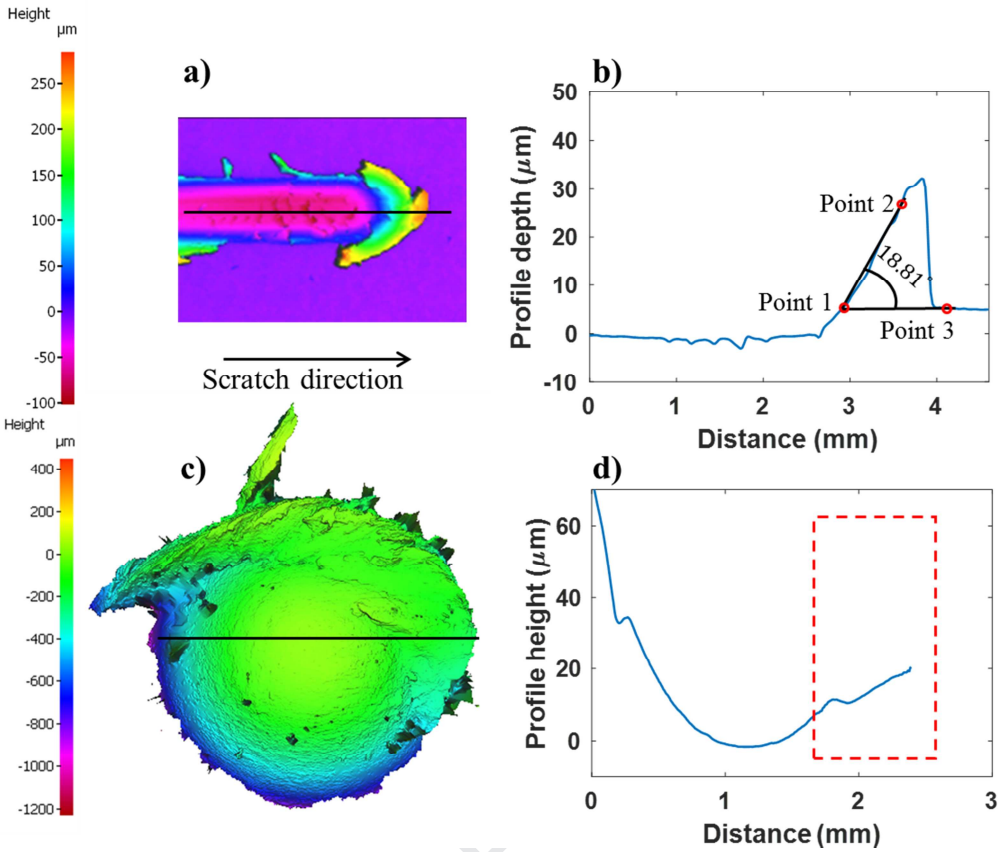

Fig. 5. a) Contour image of the scratch surface (Sliding distance=20mm, D_p=0.22) and b) the corresponding longitudinal 2D profile used for the attack angle measurement. c) Contour image of the indenter (Sliding distance=20mm, D_p=0.22) and d) the corresponding longitudinal 2D profile used to measure the position of the galling development on the indenter (highlighted area indicates the position of lump on the indenter).

2.5 Pencil lead break test

The Hsu-Nielsen pencil lead break test was performed at the start of each test, to verify the contact between the AE sensors and the indenter and workpiece, and to examine the influence of background noise. At the start of each test, the indenter was indented into the workpiece and the pencil lead (2H lead of 0.5 mm diameter) was broken against the conical region of the indenter and against the workpiece at the region close to the indenter tip. From Fig. 6 a-d, it is evident that the amplitude of the AE burst signal caused by the pencil lead event is very large compared to that of background noise (0.03 V), showing that the effect of background noise on the AE sensor is minimal. If the AE amplitude was not similar during each pencil lead break test, then the AE sensor was unclamped and fresh couplant was applied to the AE sensor face. However, it can be observed that the amplitude of the AE burst signals in Fig. 6 b-c are small compared to that of AE burst signal observed in Fig. 6 a and d. This indicates that not all events that occur on the indenter may be captured on the AE sensor placed on the workpiece and vice-versa. This may be attributed to the attenuation of the AE signal at the indenter-workpiece interface and due to the distance between two AE sensors [28-29]. Therefore, two AE sensors are required to understand the wear events taking place on the indenter and workpiece. Before the start of each scratch test, high pressure air was blown over the workpiece-indenter area to remove possible traces of the broken pencil lead.

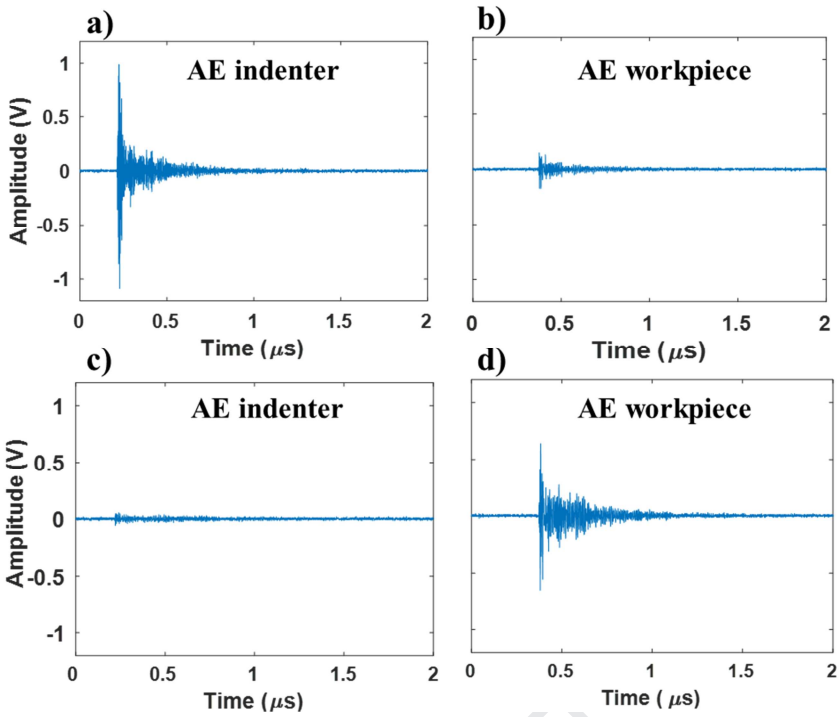

Fig. 6. Example AE measurement of a pencil lead break tests for pencil lead break on: the indenter, detected on the a) indenter, b) workpiece; and pencil lead break on the workpiece, detected on the c) indenter, d) workpiece.

2.6 AE signal during the scratch tests

To understand the AE signal related to non-galling and galling conditions (Test Set 1), the AE signal was acquired from the AE sensor placed on indenter and workpiece at different D_p. The start and end of the AE signal were identified based on the tangential force, which is shown in the results section. The absolute peak feature from these AE signals was later used to correlate with the profile depth measurement wear measurement. To correlate the AE peak with the wear index feature, the maximum AE peak was calculated for the 5 mm scratch length intervals corresponding to the position of the wear index measurement on the scratch (Fig. 2).

3. Experimental results

3.1. Results of scratch test performed at different depth of penetration (Test Set 1)

3.1.1. Indenter surface measurement

3.1.1.1 Using Optical profilometer

Fig. 7 shows the surface contours of the 3D profilometry measurements of the indenter tips after the scratch tests, prior to any cleaning of the indenter. It is evident that only debris was observed on the indenter for the D_p of 0.16, 0.18 and 0.20 (Fig. 7 a-c). This was confirmed by squirting ethanol on the indenter tip after taking the profilometer image, where the small debris particles evident in Fig. 7 a-c were washed away due to the action of the ethanol. For the D_p of 0.22, 0.24 and 0.26, galling was observed on the indenter (Fig. 7 d-f). This was confirmed by squirting ethanol on the indenter tip after taking the profilometer image. In these cases, the lump of material on the indenter remained adhered to the indenter tip. Based on this observation, the tests with D_p of 0.16, 0.18, 0.20 are considered as non-galling conditions, while the tests with D_p of 0.22, 0.24, 0.26 are considered as galling conditions.

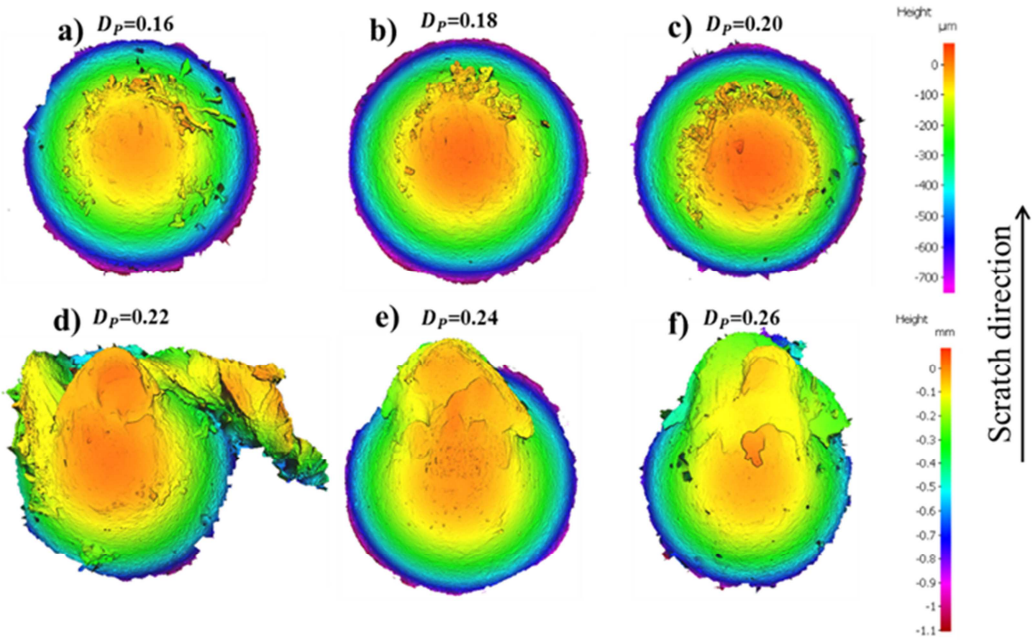

Fig. 7. Optical profilometer measurements of worn indenter after the tests for D_p: a) 0.16, b) 0.18, c) 0.20, d) 0.22, e) 0.24, f) 0.26.

3.1.1.2 Using SEM and EDX

Fig. 8 a-b shows SEM images of the galling lump from the indenter tip from Repeatability Test 1. Fig. 8a shows the entire galled lump that was accumulated on the indenter tip. From Fig. 8b, the possible agglomeration of debris material in lump can be observed. In the EDX analysis (Fig. 8c), the presence of high amount of Fe (72.57 %) indicates the transfer of sheet material on the indenter tip. In addition, the high content of O (21.98 %) presented on the galled lump can be attributed to oxidation.

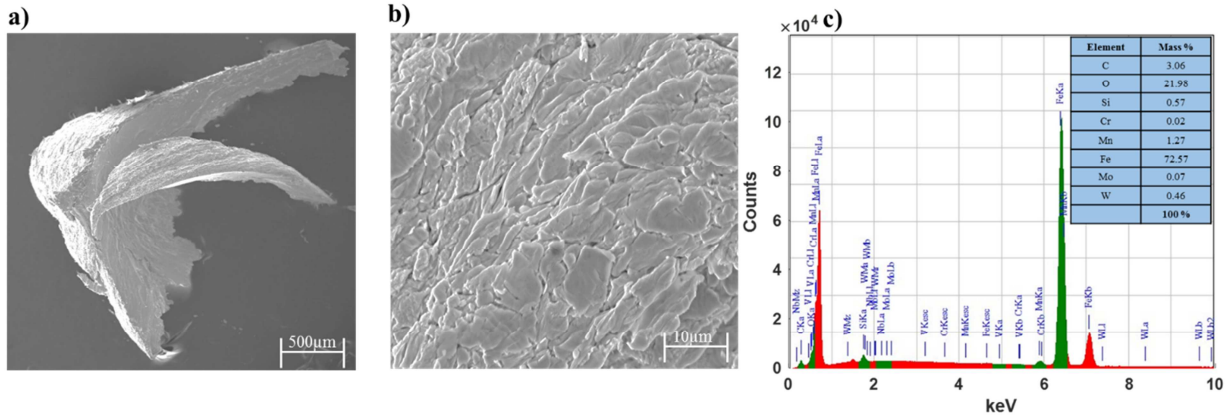

Fig. 8. SEM image of galling lump from Repeatability Test 1 (D_p 0.24) at a) 500 µm resolution b) 10 µm, and c) EDX analysis.

3.1.2. Workpiece surface measurement

For the tests with D_p of 0.16, 0.18 and 0.20, there was very little variation in the profile depth at the centre and sides of the scratches (Fig. 9 a-c). This indicates only ploughing wear mode on the sheet. For the tests with D_p of 0.22, 0.24 and 0.26, the variation in profile depth was observed at the centre and at the sides of the scratches (Fig. 9 a-c). This variation of the profile depth at the edges of the scratch was observed to initiate much earlier than at the centre of the scratch. This variation of profile depth at the edges is due to cutting wear at edges and the variation of profile depth at the centre is due to fracture at the centre of scratch (as can be seen in Fig. 2c).

Journal Pre-proof

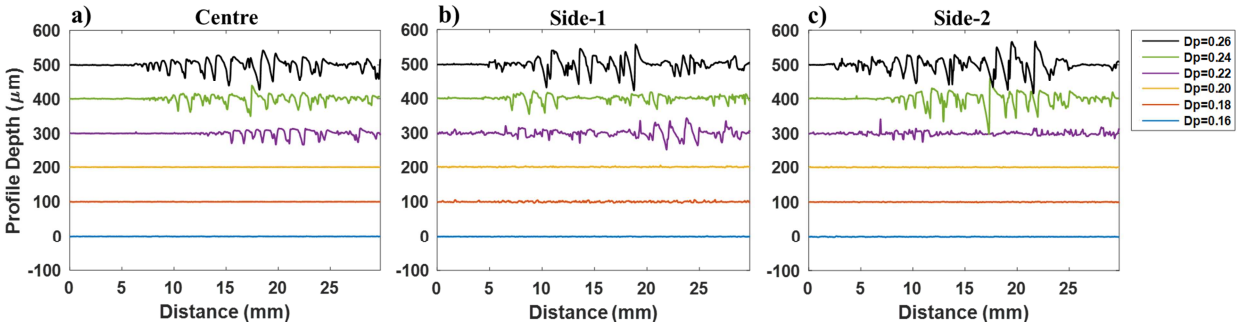

Fig. 9. Profile depth along scratch at different D_p measured at: a) centre, b) Side-1, c) Side-2. Note that each profile has been offset by +100µm from the previous profile for clarity.

Fig. 10 a-b shows the wear index calculated from the transverse surface profiles on the workpiece obtained from Test Set 1 and the Repeatability Tests. For all the tests, the wear index was observed to be less than 0.1 at the instances where only ploughing conditions or cutting at the edges were observed. The wear index was greater than 0.1 at that instances where fracture was observed at the centre of scratch – i.e. for the tests of D_p=0.22, 0.24 and 0.26. Based on these results, the wear index is greater than 0.1 for galling conditions and less than 0.1 for the non-galling conditions. The trends in the wear index measurements for the Repeatability Tests compared to the tests for D_p 0.18 and D_p 0.24 (Fig. 10) showed good test-to-test repeatability. In particular, the results for the D_p 0.18 condition showed very good consistency across all four tests. Some variation in the wear index was evident between each of the corresponding sets of wear index measurements for D_p 0.24, which corresponds to conditions where the wear index is larger – i.e. greater than ~0.1. This variation in the wear index measurement is expected due to the inherent variation of the grooves and ridges in the scratch surface as a result of the fracture and cutting mechanisms that were found to occur (as also identified in Fig. 3b).

Fig. 11 a-b shows the wear index measurement using the transverse surface profile width of 2.5 and 5mm from the test D_p 0.24. The wear index trend obtained from the average transverse profile over the 2.5 and 5 mm scratch length intervals (Fig. 11) showed good correlation in the trend of the wear index measurement, thus showing good measurement-to-measurement repeatability.

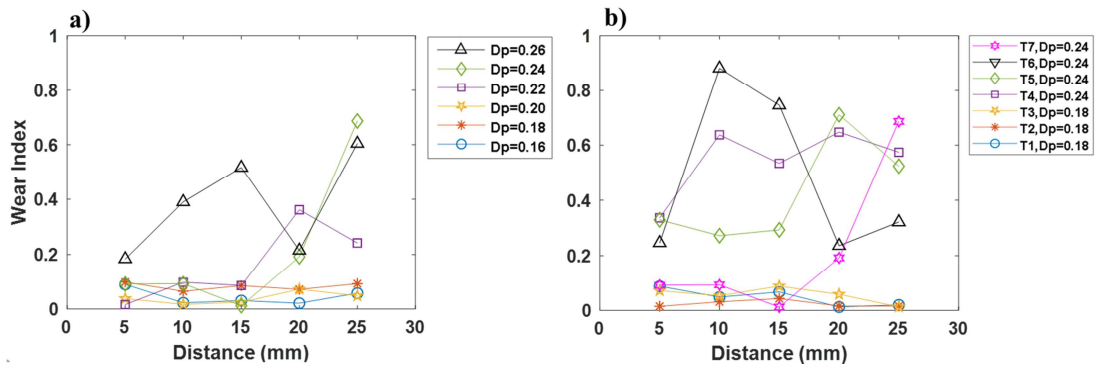

Fig. 10. a) Wear index measured from profilometry measurements of scratches from a) Test Set 1 b) Repeatability Tests (T1, T2 and T3 performed at D_p 0.18; T4, T5, T6 and T7 performed at Dp 0.24)

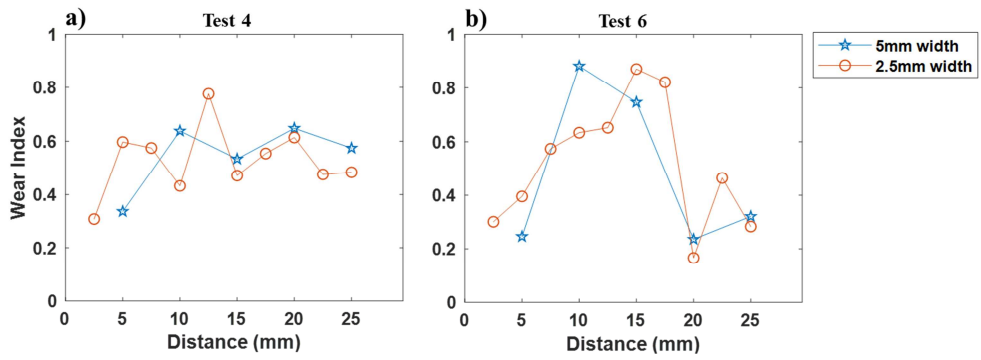

Fig. 11 : Wear index measured from profilometry measurements of scratches from Repeatability Tests performed using transverse profile width of 2.5 and 5mm for a) Test 4 b) Test 6 (Test 4 and 6 are performed at D_p 0.24)

3.1.3. Study of indenter and workpiece profile to measure galling

The methodology to measure the longitudinal profiles on the indenter and workpiece and subsequently estimate the attack angle has been explained in Section 2.4.3. Fig. 12 represents the profile of the indenter and workpiece for each test performed at varying D_p. For all the tests, the location of debris and galling on the indenter begins at approximately the same location near the tip of the indenter, as indicated in the Fig. 12-a. The indenter profile significantly changes for the galling conditions compared to that of the non-galling conditions and the increasing size of the lump of adhered material is evident with increasing D_p (Fig. 12-a). Similarly, the profile of the scratch measured at the end of scratch surface changes significantly for the galling conditions compared to that of the non-galling conditions (Fig. 12-b). The attack angle of the indenter measured from the surface profiles (Fig. 12-b) for the non-galling conditions (D_p=0.16, 0.18 and 0.20) is quite consistent (9.9º, 10.0º and 11.4º, respectively). For the galling conditions (D_p=0.22, 0.24 and 0.26), the attack shows large variation (6.6º, 4.6º and 18.8º, respectively). This will be discussed further in Section 0. However, it is worth noting that, due to the inconsistent surface caused by the lump of adhered material for $D_p \geq 0.22$, the angle of attack measurement is also inconsistent.

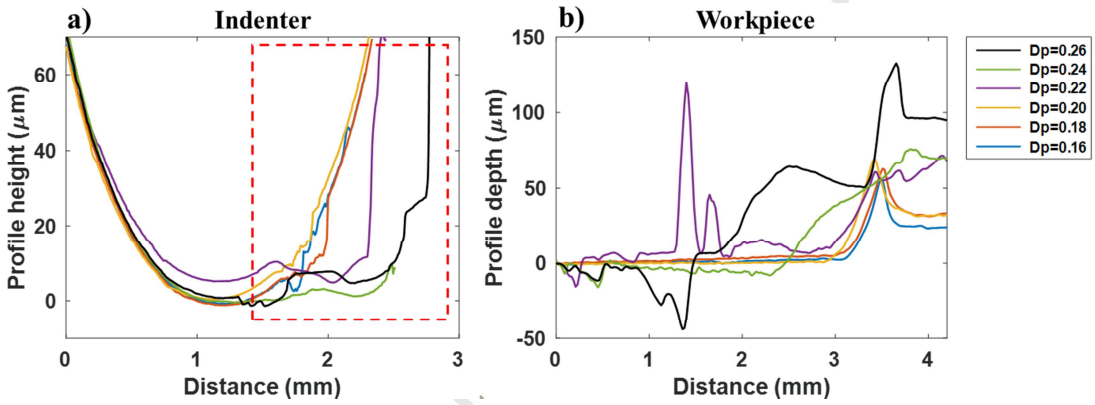

Fig. 12. The longitudinal 2D surface profile of the a) indenter and b) workpiece for Test Set 1 (varying D_p). Highlighted area indicates the position of lump on the indenter.

3.1.4. AE signal

The AE signal acquired during the scratch test for Test Set 1 and the Repeatability Test is presented in Fig. 13 and Fig. 14. For the tests performed for D_p 0.16, 0.18 and 0.20, AE burst signals were not observed from the AE sensor placed on the indenter and only a small number of AE burst signals of low amplitude were observed from the AE sensor placed on the workpiece (Fig. 13 a-c). Similarly, in the repeatability test performed for D_p 0.18, AE burst signal were not observed from the AE sensor placed on the indenter (Fig. 14 a-c). These low amplitude AE burst signals observed from AE sensor placed on workpiece are due to plastic deformation of the workpiece during the scratch test [13]. For the tests performed for D_p of 0.22, 0.24 and 0.28, large amplitude AE signals were observed from the AE sensor placed on the indenter and workpiece (Fig. 13 d-f). Similarly trend was also observed in the repeatability test performed for D_p 0.24 (Fig. 14 d-f). This indicates the presence of significant wear or fracture events on the indenter and workpiece. The amplitude of the AE burst signals and number of AE bursts observed from the AE sensor placed on the indenter is much larger than those from the AE sensor placed on the workpiece (Fig. 13 d-f).

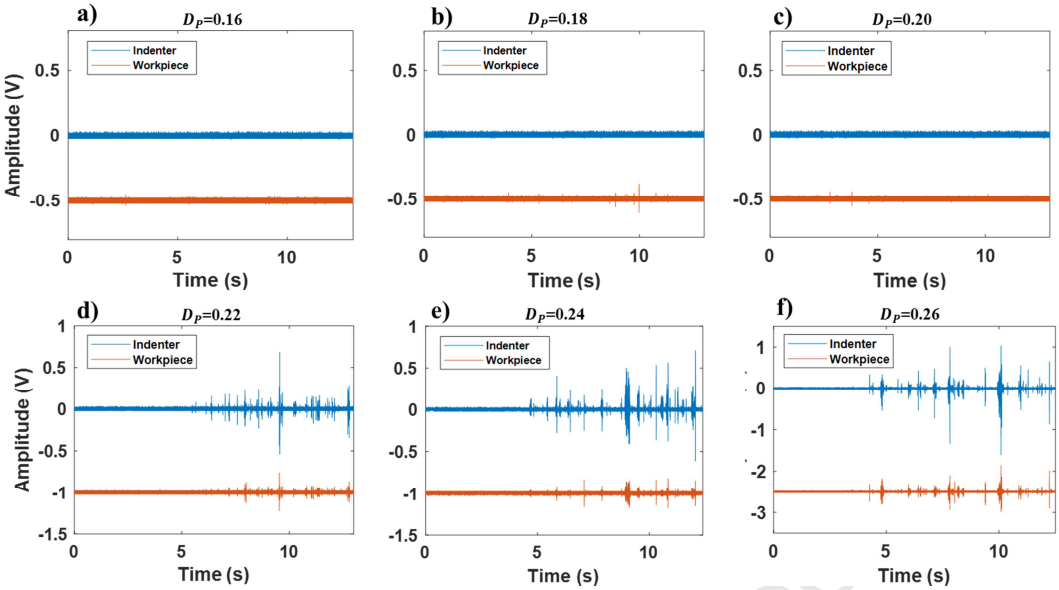

Fig. 13. AE signal from the scratch test for Test Set 1 for D_p: a) 0.16, b) 0.18, c) 0.20, d) 0.22, e) 0.24, f) 0.26. Note that workpiece signal has been offset in the negative amplitude direction for clarity.

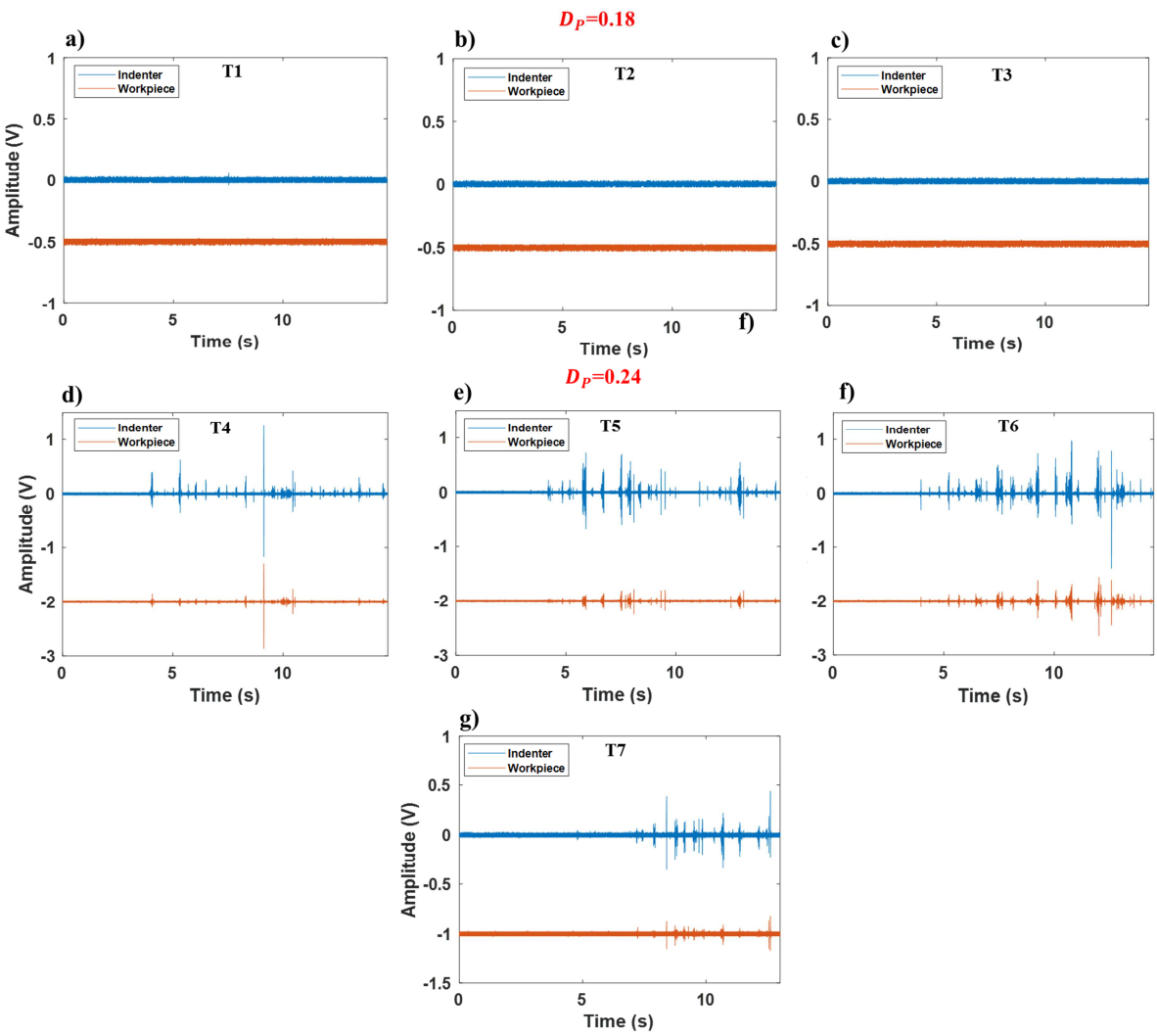

Fig. 14. AE signal from the Repeatability scratch tests for D_p 0.18 a) Test 1 b) Test 2 c) Test 3; for Dp 0.24 d) Test 4 e) Test 5 f) Test 6 (Note that workpiece AE signal has been offset in the negative amplitude direction for clarity; T1, T2 and T3 performed at D_p 0.18; T4, T5, T6 and T7 performed at D_p 0.24)

3.1.5. Correlation of tangential force and AE peak feature

Fig. 15 shows the measurements of tangential force and AE peak feature from Test Set 1. The tangential force was observed to be stable for D_p of 0.16, 0.18 and 0.20 (Fig. 15-a). No AE burst signal was observed during these tests from the AE sensor mounted on the indenter (Fig. 15-b). For the tests with D_p of 0.22, 0.24 and 0.26, an increase in tangential force was observed for a certain distance which was then followed by an unstable tangential force (Fig. 15-a). AE burst signals were not observed during the region where the tangential force was increasing. The instance at which the force variation is observed, strongly correlates with the initiation of the AE burst signal (Fig. 15-b). This can also be confirmed from the Repeatability Tests where strong correlation was observed between force variation and AE burst signal (Fig. 16 a-b). It is worth noting that, in the Repeatability Tests, all the AE burst signals and fluctuation in the tangential force start at approximately the same instance (Fig. 16 a-b). However, in Test 7 performed at D_p of 0.24, the variation in force and AE peak begins much later compared to Tests 4, 5 and 6. This is likely due to the behaviour of galling growth – i.e. the distinct initiation and rapid growth of lump [8] – and the inherent stochastic nature of mechanical wearing processes. However, it is worth noting that, the tangential force and AE peak feature can be used to understand non-galling and galling conditions. To understand if these sensors can be used to determine the point at which galling initiates, the force and AE peak data is further investigated for the experiments in Test Set 2.

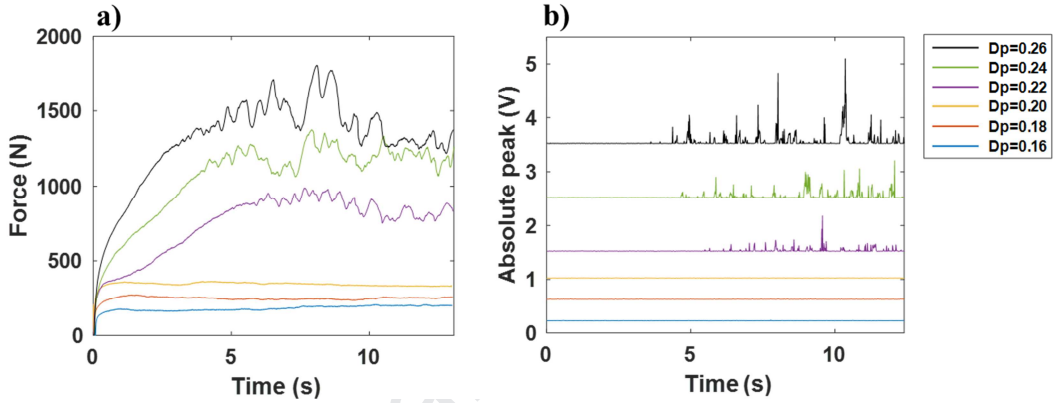

Fig. 15. a) Tangential force measurements for Test Set 1. b) The absolute AE peak on the indenter for Test Set 1 (Note that AE peak signal has been offset in the positive amplitude direction for clarity)

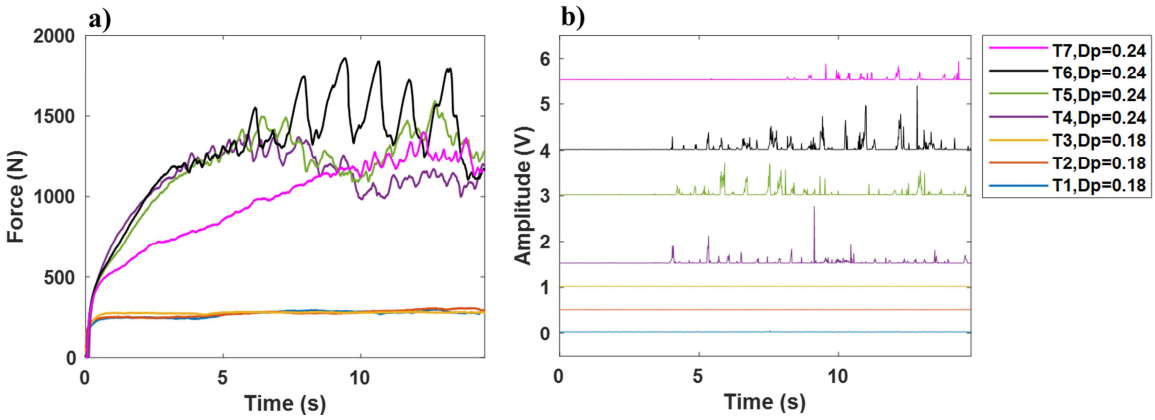

Fig. 16. a) Tangential force measurements for the repeatability experiments b) The absolute AE peak on the indenter for the repeatability experiments (Note that AE peak signal has been offset in the positive amplitude direction for clarity; T1, T2 and T3 performed at Dp 0.18; T4, T5, T6 and T7 performed at Dp 0.24)

3.2. Results of scratch test performed at different sliding distances (Test Set 2)

3.2.1. Indenter surface measurements

Fig. 17 shows the profilometer measurements of the worn indenter for Test Set 2, in which different sliding distances were tested. For the tests where the sliding distance is 15 mm or less (Fig. 17 a-c), only loose debris was observed on the indenter. This was again confirmed by squirting ethanol on the indenter, which washed away the loose debris and showed that adhered material did not remain. An example of the result of this process is shown in Fig. 18. When comparing Fig. 17c to Fig. 18 to (i.e. before and after the ethanol is squirted on the indenter tip), it is evident that only the small loose debris particles are removed and the small lump of adhered

material remains. Conversely, for the tests where the sliding distance is 30 mm or more (Fig. 17 d-f), a major lump was observed on the indenter. This lump stayed intact when the ethanol was squirted on the indenter. To confirm the influence of galling on the abrasive wear modes, the volume of the lump on the indenter was measured for the Test Set 2 experiments (Fig. 19). The methodology to calculate the volume of lump on the indenter is explained in Section 2.4.2. The volume of lump on the indenter is minimal for the non-galling conditions and very high for the galling conditions. This minimal volume measurement for the non-galling conditions is due to some of the small debris particles that are captured in the measurement. A small contribution to this volume is also possibly due to minor differences and errors between the reference surface measurement of the indenter (unworn condition) and the surface measurement of the worn indenter and due to the surface fitting routine used.

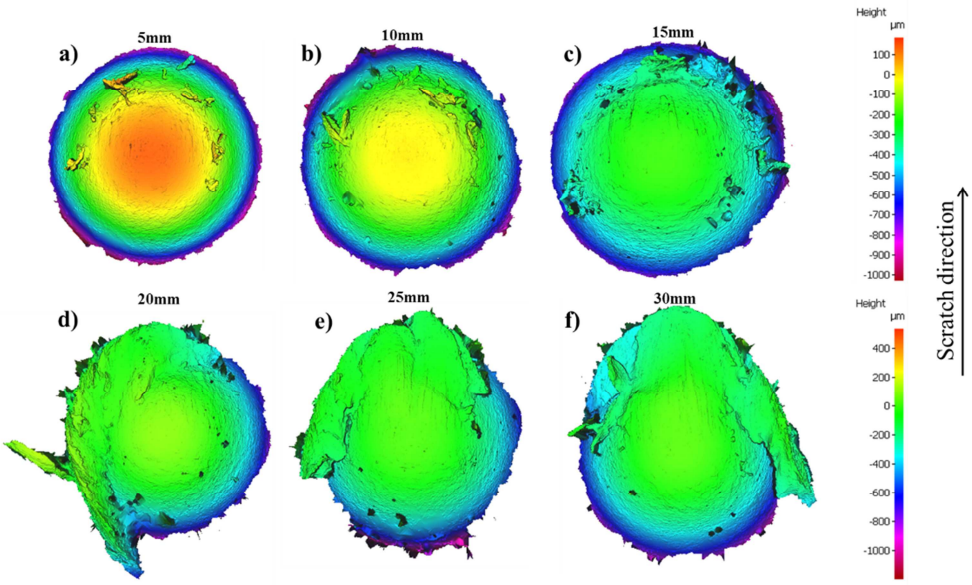

Fig. 17. Optical profilometer measurements of worn indenter after the tests for D_p of 0.22 for sliding distances of: a) 5, b) 10, c) 15, d) 20, e) 25, f) 30 mm.

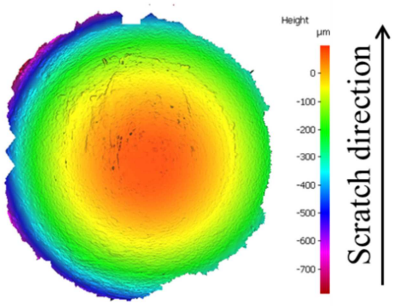

Fig. 18. Optical profilometer measurements of worn indenter after ethanol was squirted on indenter for the tests for D_p of 0.22 for the sliding distance of 15 mm.

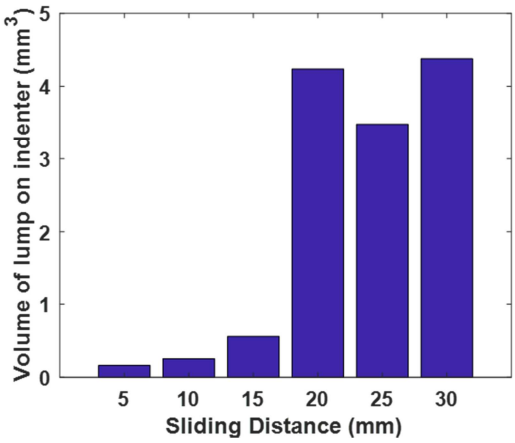

Fig. 19. Volume of additional material measured on the indenter at different sliding distance for D_p= 0.22.

3.2.2. Workpiece surface measurements

Fig. 20 shows the profile depth variation along the edges and centre of the scratches for Test Set 2. These profilometry results observed for Test Set 2 are similar to those of Test Set 1. The variation at the edges of the scratch was observed to initiate much prior to that of centre. Similar to set 1, a good correlation can be observed between the AE burst signal and profile depth as the AE burst is only observed (Fig. 23-a) when the profile depth variation is observed at the centre of scratch for 20, 25 and 30mm (Fig. 20-a). From the profilometry data from test sets 1 and 2, it can be concluded that the sequence of deformation mechanisms on the workpiece due to the increasing severity of abrasive wear modes (as D_p and/or sliding distance is increased) is: ploughing < cutting at the edges < fracture at centre.

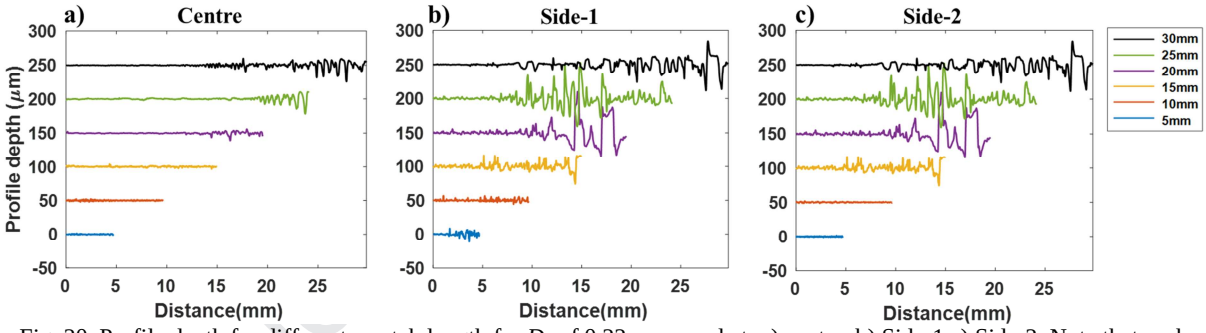

Fig. 20. Profile depth for different scratch length for D_p of 0.22 measured at: a) centre, b) Side-1 c) Side-2. Note that each profile has been offset by +50µm from the previous profile for clarity.

Fig. 21 shows the wear index calculated from the transverse surface profiles on the workpiece obtained from Test Set 2. The behaviour of the wear index is similar to that of Test Set 1 (Fig. 10), where the wear index was observed to be less than 0.1 at the instances where ploughing and cutting at the edges were observed. The wear index was greater than 0.1 at that instance where fracture was observed at the centre of scratch. For all the tests, the wear index was less than 0.1 at the start of test. However, the wear index was greater than 0.1 towards the end of the tests for sliding distances 20-30mm. This indicates that the initiation and progression of galling may play an important role on the behaviour of the abrasive wear modes (as evidenced by the increasing wear index) with increasing sliding distance.

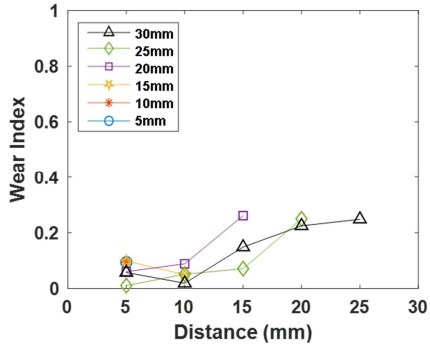

Fig. 21. Correlation of AE peak and wear index for set 2 experiments.

3.2.3. Study of indenter and workpiece surface to measure galling.

Fig. 22 shows the longitudinal profile of the indenter and workpiece for each test performed at varying sliding distance. Similar to the tests performed for set 1, the location of debris and galling on the indenter begins at approximately the same location for the test performed for set 2 as indicated in the Fig. 22-a. The indenter profile significantly changes when the galling is observed on the indenter for the 20-30mm sliding distances. Similarly, the profile of the scratch measured at the end of scratch surface increases for the galling conditions compared to that of the non-galling conditions (Fig. 22-b). The attack angle of the indenter measured from the surface profiles (Fig. 22-b) for the sliding distances of 5, 10 and 15mm is nearly consistent – i.e. 13.1º, 12.6º and 13.35º, respectively. For the sliding distances of 20, 25 and 30mm, the attack angle is varied – i.e. 18.8º, 13.34º and 20.7º, respectively. Similar to Test Set 1, it is worth noting that, due to the inconsistent surface caused by the lump of adhered material for sliding distance ≥ 20 mm, the angle of attack measurement is also inconsistent.

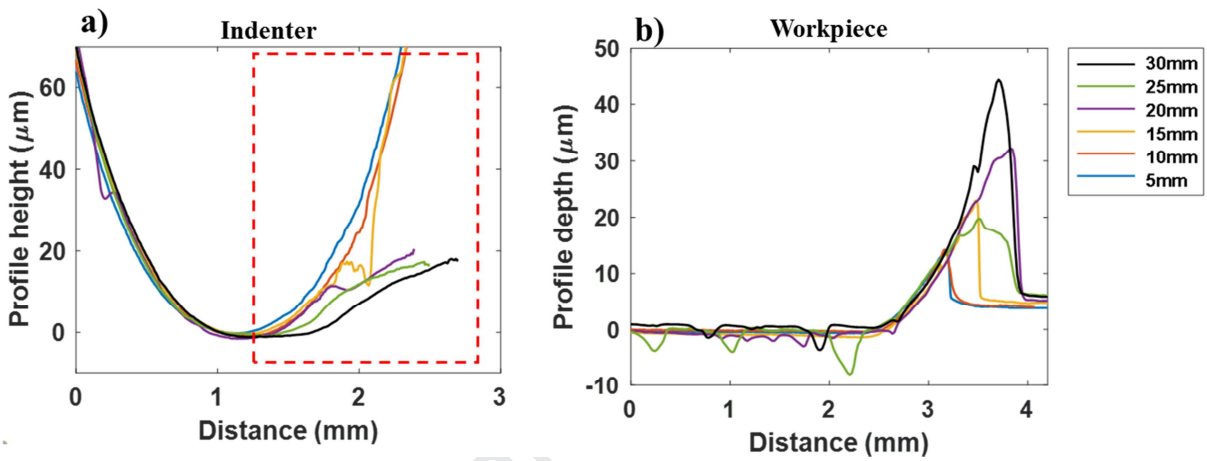

Fig. 22. The longitudinal 2D surface profile of the a) indenter and b) workpiece for Test Set 2 (varying sliding distance). Highlighted area indicates the position of lump on the indenter.

3.2.4. AE signal

The AE signal acquired during the scratch tests for Test Set 2 is presented in Fig. 23. For the scratch test performed at sliding intervals of 5-15 mm (D_p = 0.22), AE burst signals were not observed from the AE sensor placed on indenter. However, AE burst signals of low amplitude were observed from the AE sensor placed on the workpiece. This behaviour of the AE signal is similar to that of non-galling conditions from the set 1 experiments. The large amplitude AE burst signals were observed from the AE sensors placed on the indenter and workpiece at sliding distance intervals of 20, 25 and 30 mm (D_p = 0.22). Similar to set 1 experiments for the galling conditions, the amplitude of the AE burst signals and number of AE bursts measured from the AE sensor placed on indenter is larger compared to those of the AE sensor placed on the workpiece.

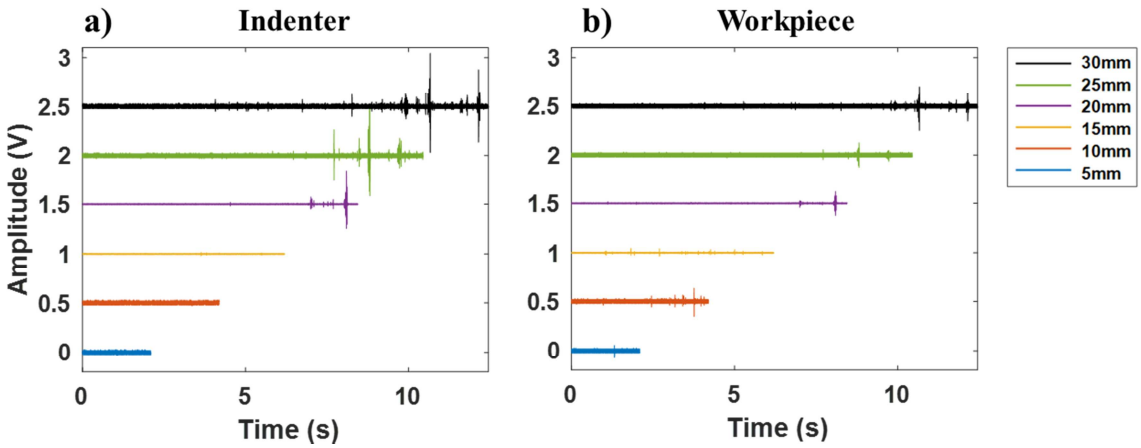

Fig. 23. AE signal for indenter and workpiece for D_p of 0.22 at different sliding distances for AE sensor placed on a) Indenter b) Workpiece. Note that each signal has been offset by +0.5V from the previous signal for clarity.

3.2.5. Correlation of tangential force with AE peak feature

Fig. 24 shows the tangential force and AE peak feature measured from Test Set 2. The tangential force was observed to increase from the start of the tests and, in general, continue to increase with increasing sliding distance. Similar to Test Set 1, there is a strong correlation between the time at which a variation is observed in the tangential force and the presence of the AE burst signal.

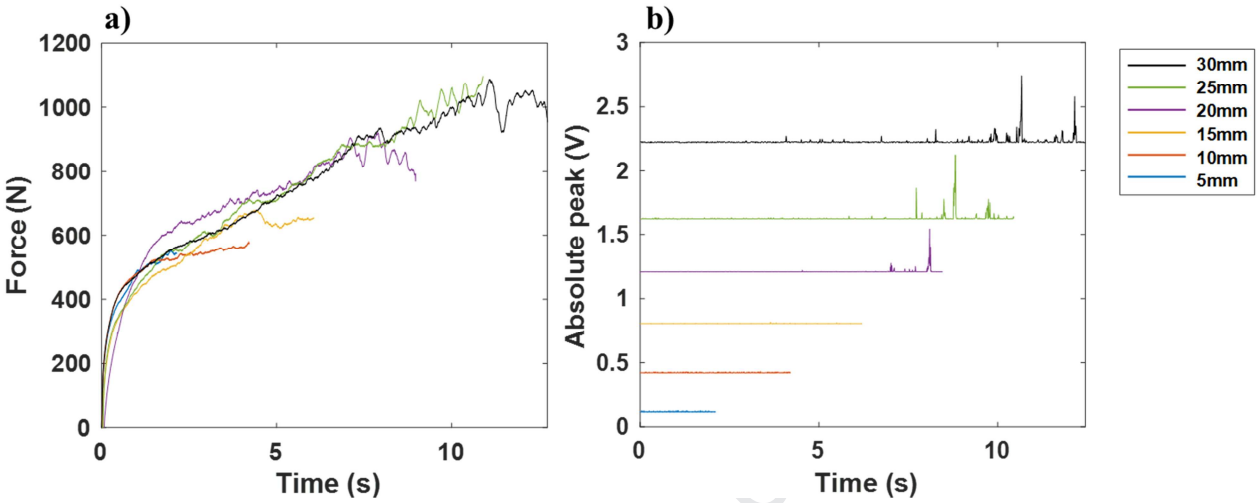

Fig. 24. a) Tangential force for set 2 experiments. b) The absolute peak for set 2 experiments

3.3. Relationship between wear index and indenter attack angle and AE peak

Fig. 25 shows the correlation of wear index with the AE peak measured at the last position (Fig. 2) at the end of the scratch for the set 1 and set 2 tests. For the tests performed at varying D_p, when the wear index is less than 0.1, the AE peak is also less than 0.1 V. This indicates that, for the non-galling conditions, the AE burst signal is not observed (Fig. 25-a). The AE burst signal is mainly observed when the wear index is greater than 0.1 (Fig. 25-a). This relationship between the behaviour of the wear index with the AE peak for non-galling and galling conditions, can be validated from the test performed at varying sliding distance (Fig. 25-b).

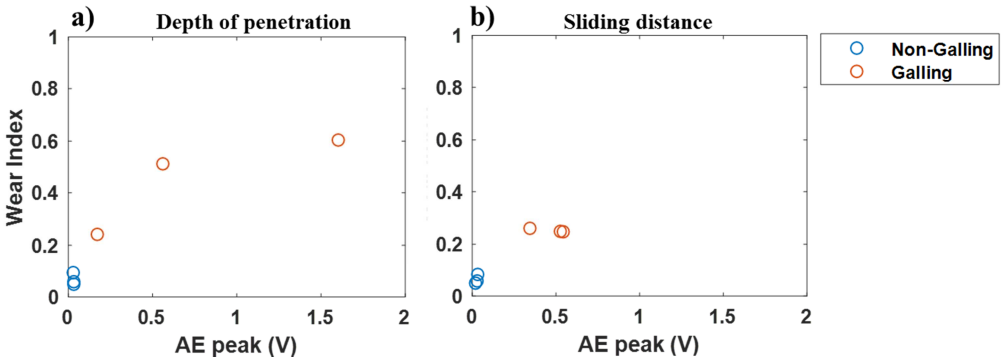

Fig. 25. Correlation of wear index with AE peak for varying a) depth of penetration (Test Set 1) and b) sliding distance (Test Set 2).

Fig. 26 represents the correlation of wear index with the attack angle measurement measured towards the end of the scratch for the set 1 and set 2 tests. For the test performed at varying D_p, when the wear index is less than 0.1, the attack angle is in range of 10-12º. The attack angle varies mainly when the wear index value is greater than 0.1 (Fig. 26-a). Similar correlation of wear index with the attack angle measurement can be validated from the test performed at varying sliding distance (Fig. 26-b).

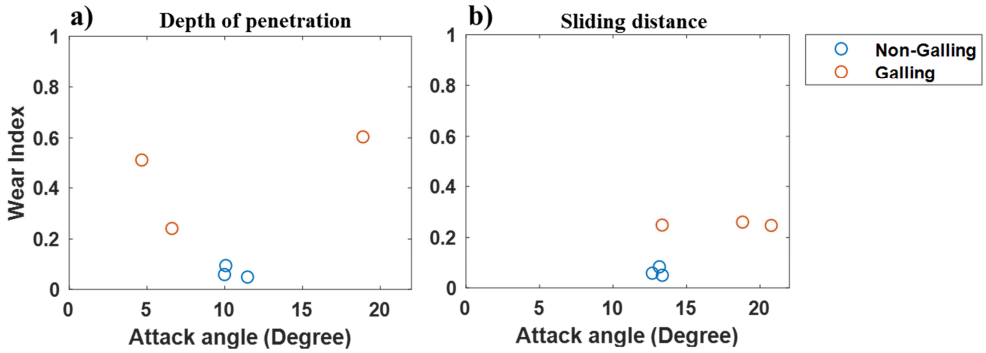

Fig. 26. Correlation of wear index with attack angle for a) depth of penetration b) sliding distance

4. Discussion

Fig. 27 aims to summarise the important features and values of the measured parameters at the end of test sets 1 and 2, which help to show the findings from this work, based on the results presented in Section 3. In particular, the conditions for non-galling, galling and the transition from non-galling to galling are evident.

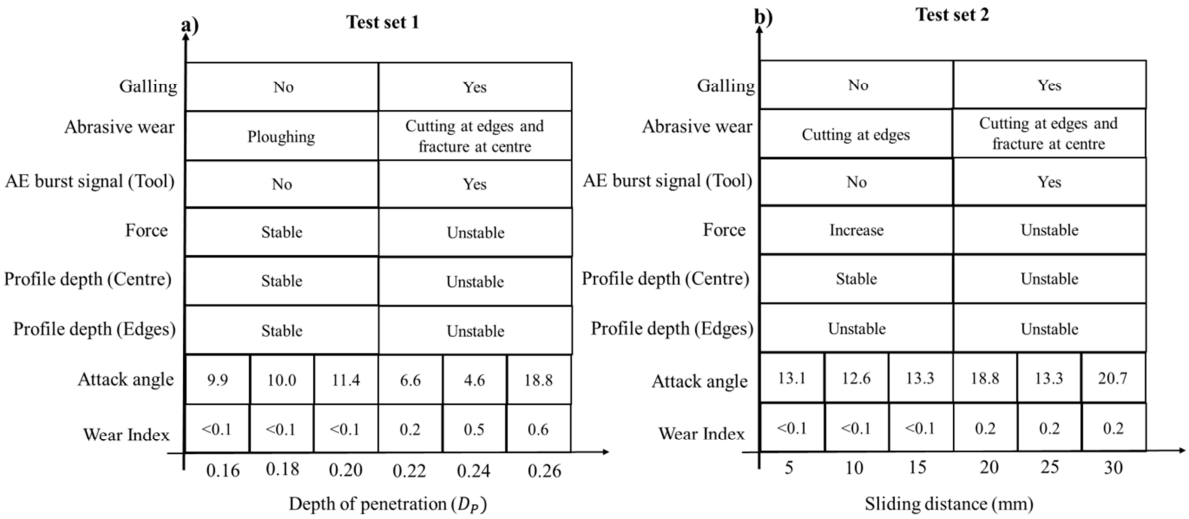

Fig. 27: Summary of results measured at the end of the tests for: a) Test Set 1 (constant sliding distance of 30 mm with varying D_p) and b) Test Set 2 (constant D_p of 0.22 with varying sliding distance).

4.1. Non-galling conditions

Fig. 27 highlights that the AE burst signal on the indenter is not observed where galling is not observed. Additionally, for the non-galling conditions (D_p=0.16, 0.18 and 0.20) only ploughing wear mode is observed. This can be also confirmed by the wear index value which is less than 0.1, which correlates well with the wear index value expected during the ploughing abrasive wear mode [24]. For the non-galling conditions, when the ploughing wear modes are observed, there is very little profile depth variation at the edges and at the centre (i.e. the profile depth is stable). Similarly, the tangential force behaviour is also stable and the AE burst signal is not observed. The stability of tangential force behaviour for the non-galling conditions can be confirmed from the work of Heidi et al. [30]. This is mainly attributed to the absence of the lump at front of the indenter, which can be confirmed from the indenter profile (Fig. 12-a) for the non-galling conditions. This can be further validated by the attack angle measurement for the non-galling conditions where the attack angle is in the range of 9-11° (Fig. 27-a). We can also note that, the profiles of the indenter (Fig. 12-a) and the profiles at the end of the scratch (Fig. 12-b) for the non-galling conditions are very consistent. Due to the low attack angle of the indenter, there is no galling on the indenter and only ploughing wear mode is observed on the workpiece, therefore the AE burst signal is not observed here (Fig. 28-a). From this analysis, it can be concluded that, for the non-galling conditions: the wear index feature as less than 0.1; the profile depth variation at edges and centre as stable; the tangential force is stable; and the AE burst signal is not observed.

4.2. Galling conditions

Fig. 27 shows that the AE burst signal is observed only for the conditions where galling is observed. For these galling conditions (D_p=0.20, 0.22 and 0.24; sliding distance=20, 25 and 30mm), the variation in profile depth at the edges and at the centre was observed. The variation of profile depth at the edges and at centre of the scratch is mainly due to cutting at the edges and fracture at the centre of scratch. This can be confirmed from the wear index measurement which is observed to be greater than 0.1 for these conditions, indicating that the wear mode on the workpiece is no longer pure ploughing [24]. This transition in the abrasive wear mode from ploughing to cutting on the workpiece is mainly due to the galling wear experienced on the indenter – i.e. due to the build-up of the lump at the front of the indenter. This can be confirmed by measuring change in attack angle of the indenter due to galling which varies significantly compared to that of non-galling conditions (Fig. 27 a-b). This can also be validated by observing the significant volume of lump on the indenter (Fig. 19), variation in indenter profile (Fig. 12-a and Fig. 22-a) and variation in scratch profile measured at the end of scratch (Fig. 12-b and Fig. 22-b). The wide variation observed in indenter attack angle for the galling conditions may be due to the variation in volume of lump on the indenter (Fig. 19) and the inconsistent shape of the galling observed on the indenter (Fig. 12-a, Fig. 22-a). According to Schedin et al. [31], when the lump at the indenter front end reaches a critical size, large amount of lump transfers to the indenter. This variation in volume and shape of the transferred lump on the indenter may have contributed to the change in scratch profile towards the end of the tests (Fig. 12-b, Fig. 22-b), resulting in the wide variation of indenter attack angle (Fig. 27 a-b).

For the galling conditions (D_p=0.20, 0.22 and 0.24; sliding distance=20, 25 and 30mm), the tangential force is unstable and high amplitude AE burst signals are observed. This lump stores a huge amount of the deformation energy. When the magnitude of the stress of the lump reaches the yield strength, the deformation energy is released in form of AE burst signal due to plastic ploughing [19]. In addition, as observed from Fig. 19, the volume of lump may not increase with increase in sliding distance (after 20mm). Therefore, it is likely that the fracture of lump takes place resulting in AE burst signals [31]. Additionally, as shown in Fig. 28-c, due to change in attack angle of the indenter, it result in a transition from ploughing to fracture at the centre of the scratch surface and results in AE burst signals. Therefore, for the galling conditions, we can define the wear index feature as greater than 0.1, profile depth variation at edges and centre as unstable, tangential force as unstable and AE burst signal is observed.

4.3. Transition of non-galling to galling conditions.

From Fig. 27 a-b, the AE burst signal was not observed when the cutting wear was observed at the edges of scratch. During the transition of non-galling to the galling conditions, the variation of profile depth was only observed at the edges of scratch and not at the centre. In this study, when the cutting wear was observed at the edges of scratch (wear index <0.1), an increase in tangential force was observed. Podgornik et al. [11] attributed the increase in tangential force to the galling wear initiation and de Rooij et al. [22] observed the galling initiation in the wedge formation wear mode. However, in this study, a minimal lump was observed on the indenter surface (Fig. 17 a-c and Fig. 19). This indicates the increase in tangential force is mainly due to the influence of D_p during this process and not mainly due to galling on the indenter. This can be confirmed from the consistency of the attack angle measurement (12-13 degrees) on the workpiece surface at the end of the scratches for Test Set 2. The increase in attack angle observed during the transition of non-galling to galling conditions, compared to that of the non-galling conditions, is because the lump accumulates at the indenter front end and it is not adhered to the indenter. The non-adhered lump is likely to remain at the scratch end resulting in the increase in attack angle measurement (Fig. 27-b). However, this lump at the indenter front causes the cutting wear at the edges of scratch. As the lump does not adhere to the indenter, the AE burst signal is not observed here (Fig. 28-b). The results represented in Fig. 27 indicate tangential force and profile depth variation at the edges can be used as features to study the prior indication of galling development on the indenter and to understand the transition from the non-galling to galling conditions.

Journal Pre-proof

Journal Pre-proof

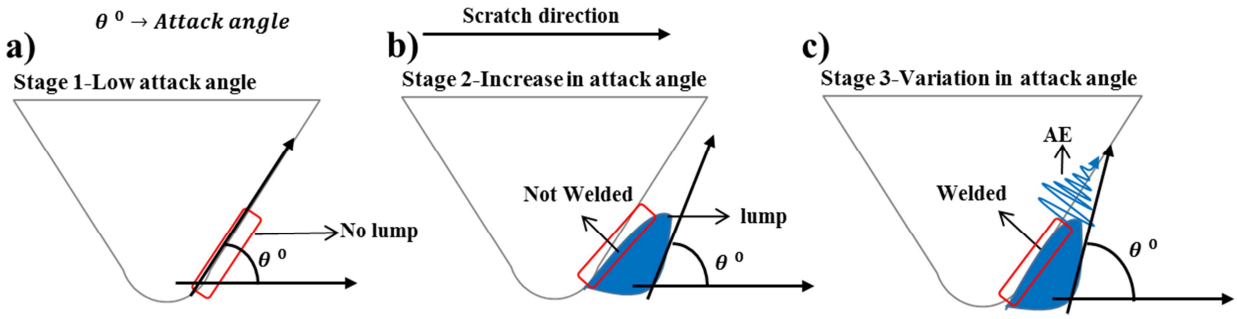

Fig. 28. Influence of galling on AE burst signal.

5. Conclusion

This work investigated the transition from non-galling to galling conditions using force, AE and profilometry wear measurements for scratch test conditions. The tests were performed at different depths of penetration and different sliding distances. The following conclusions can be made:

1. The non-galling conditions were observed for D_p less than 0.20. Only ploughing wear was observed for the non-galling conditions, which is due to the low indenter attack angle (less than 13 degrees) observed during these conditions. The presence of only ploughing wear during the non-galling conditions was validated by the wear index measurement that was less than 0.1 and the longitudinal profile depth measurement along the edges of the scratch that was stable.
2. For the non-galling conditions, the tangential force was stable and AE burst signals were not observed on the workpiece or indenter.
3. Galling was observed on the indenter when the D_p was more than 0.22. For these galling conditions, cutting and fracture was observed on the workpiece. The presence of fracture is due to the increase in attack angle of the indenter, which was a combined effect of the higher *Dp* and the lump of galled material at the front of the indenter. The presence of fracture during the galling conditions was validated by wear index measurement that was greater than 0.1 and the longitudinal profile depth measurement along the edges of the scratch that was observed to be unstable.
4. For the galling conditions, the tangential force was observed to be unstable, and of higher magnitude than the non-galling conditions. Additionally, for the galling conditions the AE burst signal was present.
5. During the transition from non-galling to the galling conditions, the abrasive cutting wear mode was observed. Corresponding to the area of cutting at the edges, an increase of tangential force was observed. This cutting at the edges is due to a change in indenter attack angle as a result of the high D_p and, due to the lump development at the indenter front end, which was not yet adhered to the indenter. This was validated by volume measurement of galling which indicated a minimal volume of lump on the indenter.
6. The transition from non-galling to galling conditions can be actively monitored by studying the initiation of unstable force and the presence of AE burst signals.

5. References:

1. Ubhayaratne, I., Pereira, M.P., Xiang, Y. and Rolfe, B.F., 2017. Audio signal analysis for tool wear monitoring in sheet metal stamping. Mechanical Systems and Signal Processing, 85, pp.809-826.
2. ASTM, A., 2013. Standard Terminology Relating to Wear and Erosion. G40.
3. Gåård, A., Krakhmalev, P.V., Bergström, J. and Hallbäck, N., 2007. Galling resistance and wear mechanisms–cold work tool materials sliding against carbon steel sheets. Tribology letters, 26(1), pp.67-72.
4. Karlsson, P., Gåård, A., Krakhmalev, P. and Bergström, J., 2012. Galling resistance and wear mechanisms for cold-work tool steels in lubricated sliding against high strength stainless steel sheets. Wear, 286, pp.92-97.
5. Challen, J.M. and Oxley, P.L.B., 1979. An explanation of the different regimes of friction and wear using asperity deformation models. Wear, 53(2), pp.229-243.
6. Pereira, M.P., Yan, W. and Rolfe, B.F., 2012. Wear at the die radius in sheet metal stamping. Wear, 274, pp.355-367.
7. Shanbhag, V.V., Rolfe, B.F., Arunachalam, N. and Pereira, M.P., 2018, September. Understanding the source of acoustic emission signals during the wear of stamping tools. In IOP Conference Series: Materials Science and Engineering (Vol. 418, No. 1, p. 012098). IOP Publishing.

8. Schedin, E., 1994. Galling mechanisms in sheet forming operations. Wear, 179(1-2), pp.123-128.
9. Abdelbary, A., 2015. Wear of polymers and composites. Woodhead Publishing.
10. Van der Heide, E., Huis, A.J. and Schipper, D.J., 2001. The effect of lubricant selection on galling in a model wear test. Wear, 251(1-12), pp.973-979.
11. Podgornik, B., Hogmark, S. and Pezdirnik, J., 2004. Comparison between different test methods for evaluation of galling properties of surface engineered tool surfaces. Wear, 257(7-8), pp.843-851.
12. Hase, A., Mishina, H. and Wada, M., 2012. Correlation between features of acoustic emission signals and mechanical wear mechanisms. Wear, 292, pp.144-150.
13. Sindi, C.T., Najafabadi, M.A. and Salehi, M., 2013. Tribological behavior of sheet metal forming process using acoustic emission characteristics. Tribology Letters, 52(1), pp.67-79.
14. Voss, B.M., Pereira, M.P., Rolfe, B.F. and Doolan, M.C., 2017. A new methodology for measuring galling wear severity in high strength steels. Wear, 390, pp.334-345.
15. Skåre, T., Thilderkvist, P. and Ståhl, J.E., 1998. Monitoring of friction processes by the means of acoustic emission measurements—deep drawing of sheet metal. Journal of Materials Processing Technology, 80, pp.263-272.
16. Shanbhag, V.V., Rolfe, B.F., Arunachalam, N. and Pereira, M.P., 2018. Investigating galling wear behaviour in sheet metal stamping using acoustic emissions. Wear, 414, pp.31-42.
17. Griffin, J. and Chen, X., 2008. Characteristics of the acoustic emission during horizontal single grit scratch tests: Part 1 characteristics and identification. International Journal of Abrasive Technology, 2(1), pp.25-42.
18. Perfilyev, V., Moshkovich, A., Lapsker, I. and Rapoport, L., 2017. Deformation and Fracture of Copper and Silicon During Indentation Acoustic Emission Measurements. Tribology Letters, 65(2), p.41.
19. Zhou, W., He, Y. and Lu, X., 2016. Scratch deformation mechanism of copper based on acoustic emission. Insight-Non-Destructive Testing and Condition Monitoring, 58(5), pp.256-263.
20. Bull, S.J. and Rickerby, D.S., 1989. Multi-pass scratch testing as a model for abrasive wear. Thin Solid Films, 181(1-2), pp.545-553.
21. Williams, J.A., 1996. Analytical models of scratch hardness. Tribology international, 29(8), pp.675-694.
22. de Rooij, M.B. and Schipper, D.J., 2001. Analysis of material transfer from a soft workpiece to a hard tool: Part I—Lump growth model. Journal of tribology, 123(3), pp.469-473.
23. de Rooij, M.B. and Schipper, D.J., 2001. Analysis of material transfer from a soft workpiece to a hard tool: part II—experimental verification of the proposed lump growth model. Journal of tribology, 123(3), pp.474-478.
24. Hokkirigawa, K., Kato, K. and Li, Z.Z., 1988. The effect of hardness on the transition of the abrasive wear mechanism of steels. Wear, 123(2), pp.241-251.
25. IF-MeasurementSuite 5.1. Retrieved on Jan 21, 2017 https://www.ita- polska.com.pl/upload/documents/IF-MeasureSuite_5.1_ProductInfo_EN1.pdf
26. MathWorks, (2015). Trapz. Retrieved on June 21, 2018 from, https://au.mathworks.com/help/matlab/ref/trapz.html
27. Gåård, A., Krakhmalev, P. and Bergström, J., 2009. Wear mechanisms in galling: cold work tool materials sliding against high-strength carbon steel sheets. Tribology letters, 33(1), pp.45-53.
28. Surgeon, M. and Wevers, M., 1999. One sensor linear location of acoustic emission events using plate wave theories. Materials Science and Engineering: A, 265(1-2), pp.254-261.
29. Sause, M.G., 2013. Acoustic emission signal propagation in damaged composite structures. Journal of Acoustic Emission, 31(1), pp.1-18.
30. Van der Heide, E. and Schipper, D.J., 2003. Galling initiation due to frictional heating. Wear, 254(11), pp.1127-1133.
31. Schedin, E. and Lehtinen, B., 1993. Galling mechanisms in lubricated systems: a study of sheet metal forming. Wear, 170(1), pp.119-130.

Journal Pre-proof

Journal Pre-proof

Highlights

- AE peak feature can be used to study initiation of galling.
- Tangential force can be used to indicate prior indication of galling.
- Indenter attack angle plays an important role on the abrasive wear transition.
- Profile depth is quantitative wear measurement to study abrasive wear transition.

Journal Pre-proof